

# Neutrino hierarchy from CP-blind observables with high density magnetized detectors

A. Donini<sup>a</sup>, E. Fernandez-Martinez<sup>a</sup>, P. Migliozzi<sup>b</sup>, S. Rigolin<sup>a</sup>, L. Scotto Lavina<sup>b,c</sup>,  
M. Selvi<sup>d</sup>, T. Tabarelli de Fatis<sup>e</sup>, F. Terranova<sup>f</sup>

<sup>a</sup> I.F.T. and Dep. Física Teórica, U.A.M., Madrid, Spain

<sup>b</sup> I.N.F.N., Sez. di Napoli, Napoli, Italy

<sup>c</sup> Dip. di Fisica, Università “Federico II”, Napoli, Italy

<sup>d</sup> I.N.F.N., Sez. di Bologna, Bologna, Italy

<sup>e</sup> Università di Milano Bicocca and I.N.F.N., Milano, Italy

<sup>f</sup> I.N.F.N., Laboratori Nazionali di Frascati, Frascati (Rome), Italy

## Abstract

High density magnetized detectors are well suited to exploit the outstanding purity and intensities of novel neutrino sources like Neutrino Factories and Beta Beams. They can also provide independent measurements of leptonic mixing parameters through the observation of atmospheric muon-neutrinos. In this paper, we discuss the combination of these observables from a multi-kton iron detector and a high energy Beta Beam; in particular, we demonstrate that even with moderate detector granularities the neutrino mass hierarchy can be determined for  $\theta_{13}$  values greater than  $4^\circ$ .

# 1 Introduction

In the standard interpretation of the experimental evidence for neutrino oscillation [1, 2], the squared-mass differences among the  $\nu$  mass eigenstates ( $m_1$ ,  $m_2$  and  $m_3$ ) are rather hierarchical:  $\Delta m_{21}^2 \equiv m_2^2 - m_1^2 \simeq 1/30 \times |\Delta m_{32}^2| \simeq |\Delta m_{31}^2|$ . The small size of  $\Delta m_{21}^2$  is implied by solar and long-baseline reactor neutrino data. In this framework, particularly enlightening are the oscillations at the “atmospheric scale”, i.e. when  $|\Delta m_{32}^2|L/4E \simeq \pi/2$ ,  $L$  and  $E$  being the neutrino energy and path-length, respectively. A muon-neutrino oscillating at the atmospheric scale undergoes mainly  $\nu_\mu \rightarrow \nu_\tau$  transitions. This dominant mode is implied by long-baseline accelerator experiments, atmospheric and short-baseline reactor data; moreover, it is currently under test in a direct manner at CNGS [3]. We have no evidence of subdominant  $\nu_\mu \rightarrow \nu_e$  transitions at such scale, implying a small mixing angle between the first and third mass eigenstate ( $\theta_{13} < 10^\circ$  at 90% C.L. [4]). If  $\theta_{13}$  is non-zero, the subdominant  $\nu_\mu \rightarrow \nu_e$  amplitude and its T or CP conjugates encode a wealth of information. In particular, it allows the determination of  $\theta_{13}$  and the Dirac complex phase of the leptonic mixing matrix. The  $\nu_\mu \rightarrow \nu_e$  transition probability is also perturbed by matter effects if the path of the neutrinos through the Earth is sufficiently large. The perturbation depends on the sign of  $\Delta m_{31}^2$  and therefore it allows the determination of the hierarchy among the neutrino masses. These considerations explain the enormous interest toward novel neutrino sources operating at the atmospheric scale [5] like, for instance, Neutrino Factories [6] or Beta Beams [7]. Combination of these facilities with more traditional measurements of atmospheric neutrinos has also been considered [8, 9, 10]. Such combination is particularly natural when the detector at the far location is dense and capable of charge reconstruction: this is the case of magnetized iron calorimeters, which can perform detailed measurements of atmospheric  $\nu_\mu$  fluxes and are recognized as ideally suited to exploit a possible Neutrino Factory or high energy Beta Beam [11, 12, 13, 14, 15]. However, it is generally believed that the contribution of atmospheric neutrinos is marginal for any realistic configuration, unless the value of the  $\theta_{13}$  angle turns out to be very close to current bounds [16]. In this paper, we carry out a more detailed analysis of the atmospheric data that can be collected by a 40-kton magnetized iron calorimeter (Sec.3). This analysis is tuned to identify the occurrence of resonant transitions in the earth and it is combined with the data that can be collected by the same detector exposed to a high energy Beta Beam [12] at a baseline of  $\sim 700$  km (Sec.4). The sensitivity of the atmospheric data to the neutrino mass hierarchy does not depend on the value of  $\delta$  (“CP-blind”) but it is highly deteriorated by the lack of knowledge of  $\theta_{13}$ ; on the other hand, the Beta Beam data exhibits a very strong dependence on  $\delta$  but provide tight constraints on the size of the  $\theta_{13}$ . Their combination (Sec. 5) results in a significantly improved capability to determine the hierarchy of the neutrino mass eigenstates.

## 2 Atmospheric and long-baseline oscillations

Current experimental data are unable to fix uniquely the hierarchy of neutrino masses [1], i.e. whether the  $m_1$  eigenstate is lighter than  $m_3$  ( $m_1 < m_2 < m_3$ : “normal hierarchy”) or heavier ( $m_3 < m_1 < m_2$ : “inverted hierarchy”). Clearly, this pattern is of great theoretical relevance because it allows discrimination among models that explain neutrino masses [17]. In vacuum, observables sensitive to the mass pattern exist but their exploitation is extremely challenging from the experimental point of view [18]. However, propagation in matter can enhance the perturbations to the transition probabilities due to the sign of  $\Delta m_{31}^2$  and, for sizable values of  $\theta_{13}$  such perturbations become observable even with present technologies. In particular, the  $\nu_e \rightarrow \nu_\mu$  transition amplitude (or its T and CP-conjugate) encodes an explicit dependence on the sign of  $\Delta m_{31}^2$  [19, 20]:

$$\begin{aligned}
P_{\nu_e \rightarrow \nu_\mu} \simeq & \sin^2 2\theta_{13} \sin^2 \theta_{23} \frac{\sin^2[(1 - \hat{A})\Delta]}{(1 - \hat{A})^2} \\
& + \alpha \sin 2\theta_{13} \xi \sin \delta \sin(\Delta) \frac{\sin(\hat{A}\Delta)}{\hat{A}} \frac{\sin[(1 - \hat{A})\Delta]}{(1 - \hat{A})} \\
& + \alpha \sin 2\theta_{13} \xi \cos \delta \cos(\Delta) \frac{\sin(\hat{A}\Delta)}{\hat{A}} \frac{\sin[(1 - \hat{A})\Delta]}{(1 - \hat{A})} \\
& + \alpha^2 \cos^2 \theta_{23} \sin^2 2\theta_{12} \frac{\sin^2(\hat{A}\Delta)}{\hat{A}^2}.
\end{aligned}$$

In this formula  $\Delta \equiv \Delta m_{31}^2 L/(4E)$  and the terms contributing to the Jarlskog invariant are split into the small parameter  $\sin 2\theta_{13}$ , the  $\mathcal{O}(1)$  term  $\xi \equiv \cos \theta_{13} \sin 2\theta_{12} \sin 2\theta_{23}$  and the CP term  $\sin \delta$ ;  $\hat{A} \equiv 2\sqrt{2}G_F n_e E/\Delta m_{31}^2$  with  $G_F$  the Fermi coupling constant and  $n_e$  the electron density in matter. Note that the sign of  $\hat{A}$  depends on the sign of  $\Delta m_{31}^2$  which is positive (negative) for normal (inverted) hierarchy of neutrino masses.

For a monochromatic beam, a  $\nu_e \rightarrow \nu_\mu$  run combined with its CP conjugate  $\bar{\nu}_e \rightarrow \bar{\nu}_\mu$  cannot determine uniquely  $\text{sign}(\Delta m_{31}^2)$  for all values of  $\delta$ . In particular, if the hierarchy is normal (inverted) and  $\delta < 0$  ( $\delta > 0$ ), it is always possible to find a solution that reproduces the correct  $\nu_e \rightarrow \nu_\mu$  and  $\bar{\nu}_e \rightarrow \bar{\nu}_\mu$  rate assuming the wrong hypothesis on  $\text{sign}(\Delta m_{31}^2)$ . For beams of finite width, spectral information help lifting this ambiguity but, in general, they require very large statistics and excellent detector resolution. Figs. 1 and 2 show the allowed  $\theta_{13}, \delta$  region from a neutrino and anti-neutrino run of a Super-SPS [21] based Beta Beam assuming both the wrong (red) and right (green) hypothesis<sup>1</sup>. The true parameters are  $\theta_{13} = 4^\circ$ ,  $\text{sign}(\Delta m_{31}^2) = +1$  and  $\delta = 90^\circ$  (Fig.1) or  $\delta = -90^\circ$  (Fig.2). The existence of overlapping regions in Fig.2 testifies the consistency of the wrong hypothesis with the accelerator data. In general, we expect a highly

---

<sup>1</sup>Details on this experimental setup are given in [12] and briefly recalled in Sec. 3.

deteriorated sensitivity to mass hierarchy for nearly 50% of the possible true values of  $\delta$ . This is clearly visible in Fig.8 of [12] and it is reproduced in Fig.6 (blue line)<sup>2</sup>.

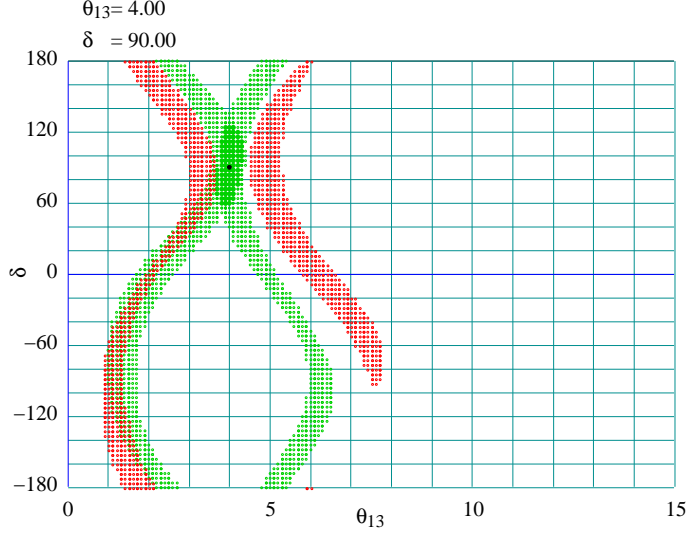


Figure 1: Allowed  $\theta_{13}, \delta$  regions from a neutrino and anti-neutrino run of a Super-SPS based Beta Beam assuming the wrong (inverted - red) and right (normal - green) mass hierarchy hypothesis. The true parameters are  $\theta_{13} = 4^\circ$ ,  $\text{sign}(\Delta m_{31}^2) = +1$  and  $\delta = 90^\circ$ .

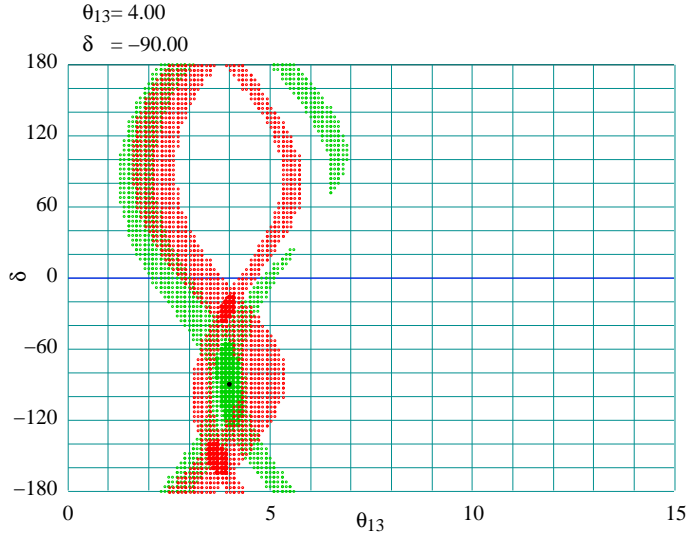


Figure 2: As in Fig. 1 with  $\delta = -90^\circ$ . Overlapping regions are present also for the wrong hypothesis (red area).

Since the dependence on  $\delta$  and, in general, the three-family interference effects are the origin of this ambiguity, a substantial improvement can be achieved exploiting CP-

<sup>2</sup>Actually, most of the next generation long-baseline experiments proposed so far suffer from this limitation. For an example based on Superbeams we refer to [22].

blind observables. In  $\nu_e \rightarrow \nu_\mu$  transitions, CP-blindness can be achieved introducing a phase advance (increase of baseline) such that the phase acquired by neutrinos due to interaction with matter equals  $2\pi$  [23]. It can be shown [24] that this condition is equivalent to choosing  $L = 2\pi/\sqrt{2}G_F n_e$ , i.e. finding a  $L$  such that the last three terms of Eq.1 cancels. Such baseline is dubbed “magic” in literature [23] and it is proportional to the energy and width of the MSW resonance in a medium of constant density:

$$E_R = \pm \Delta m_{31}^2 L_{magic} \cos 2\theta_{13}/4\pi \quad (1)$$

$$\Gamma_R = |\Delta m_{31}^2| L_{magic} \sin 2\theta_{13}/2\pi \quad (2)$$

the  $+$  ( $-$ ) sign referring to neutrinos (antineutrinos). A similar approach can be pursued using atmospheric neutrinos. In this case, however, additional difficulties are present. First of all, the initial flux is a mixture of  $\nu_\mu$ ,  $\nu_e$  and their antiparticles. Moreover, the approximation of constant density is non tenable and core-mantle interference effects are possible. Finally, the detector resolution must be sufficient to identify the region where the MSW resonance occurs. In turn, the latter condition is a requirement on the size of  $\theta_{13}$  through Eq.2. Eq. 1 implies that the resonance condition can occur only for neutrinos if the hierarchy is normal and only for anti-neutrinos if the hierarchy is inverted. Hence, the task of fixing the hierarchy is reduced to the issue of determining the occurrence of this resonance or at least the spectral perturbation induced by it in the neutrino (antineutrino) sample. Such perturbation is depicted in Fig.3 for  $\sin^2 2\theta_{13} = 0.1$  (normal hierarchy) as a function of  $L/E$  and the Nadir angle  $\theta$  of the neutrinos. It has been computed solving numerically [25] the Schroedinger equation for the propagation of neutrinos in matter and assuming the Earth density profile of Ref. [26]. For all currently allowed values of  $\Delta m_{21}^2/|\Delta m_{32}^2|$ , three family interference effects are negligible in the multi-GeV neutrino sample [16] ( $E > 1.5$  GeV) and, therefore, the observables are completely CP-blind.

### 3 Experimental setup

The experimental setup considered in this paper closely follows the configuration studied in Ref. [12]. It exploits a possible novel source operating in  $\nu_e \rightarrow \nu_\mu$  mode, i.e. a Beta Beam leveraging an upgraded injection complex for the LHC. The Beta Beams are pure sources of electron-neutrinos obtained producing, accelerating and stacking beta-unstable isotopes. The most advanced machine study regarding this novel approach is currently in progress within the Eurisol Design Study group [27]; it is based on existing CERN accelerating machines (PS and SPS) and uses  $^6\text{He}$  and  $^{18}\text{Ne}$  as  $\bar{\nu}_e$  and  $\nu_e$  emitters, respectively.

Compared with such baseline configuration, the setup of [12], which was originally proposed in Ref. [11] for a massive water Cherenkov detector, considers a higher energy proton injector to the LHC (the “Super-SPS” instead of the existing SPS) employed to increase the  $\gamma$  of the ions; in this case, the neutrinos have energies exceeding 1 GeV.

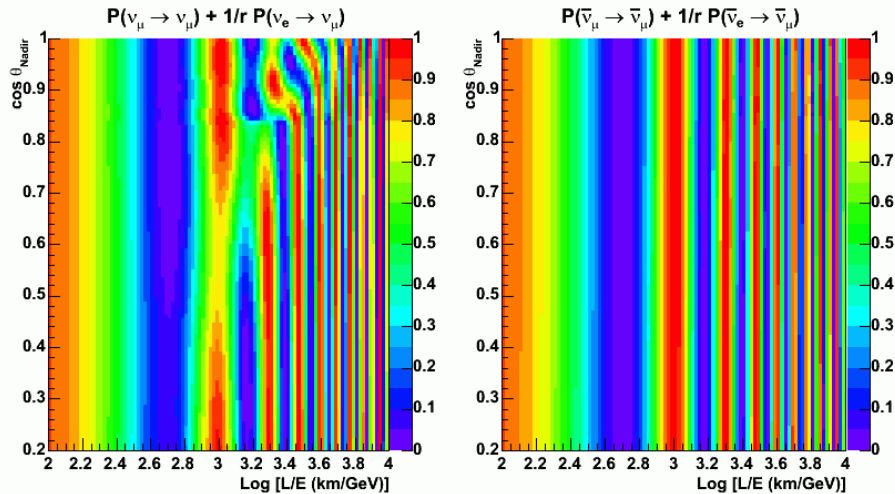


Figure 3: Probability of observing atmospheric muon neutrinos (left plot - antineutrinos are shown in the right plot) from  $\nu_\mu \rightarrow \nu_\mu$  and  $\nu_e \rightarrow \nu_\mu$  transitions as a function of  $L/E$  and the Nadir angle  $\theta$  ( $\sin^2 2\theta_{13} = 0.1$ ,  $\Delta m_{31}^2 = 2.5 \cdot 10^{-3} \text{ eV}^2$ ). In the upper label,  $r$  is the ratio between the initial  $\nu_\mu$  and  $\nu_e$  fluxes.

The corresponding spectra are recalled in Fig. 4. They are computed assuming the far detector to be located 730 km from CERN (CERN-to-Gran Sasso distance) and the ions accelerated up the same  $\gamma$  ( $\gamma = 350$ ) both for  ${}^6\text{He}$  and for  ${}^{18}\text{Ne}$  (“ $\gamma = 350, 350$  option”<sup>3</sup>) or up to the maximum rigidity allowed by the Super-SPS ( $\gamma = 580$  for  ${}^{18}\text{Ne}$ ,  $\gamma = 350$  for  ${}^6\text{He}$ ). At these energies, final state muons produced by  $\nu_\mu$  charged-current interactions have a range significantly larger than the pion interaction length in iron. Hence, muon identification against the bulk of  $\nu_e$  CC and NC interactions becomes possible even for high density iron detectors. Differently from the case of the Neutrino Factories, the far detector does not require charge identification capability: the initial state  $\nu_e$  beam is free from  $\bar{\nu}_\mu$  contaminations and  $\mu^+$  production from charm or tau decays is kinematically suppressed. In this context, the only advantage of magnetization comes from the additional suppression of the NC background with a pion misidentified as a muon.

In Ref. [12], the detector was based on glass Resistive Plate Chambers interleaved with 4 cm thick vertical iron slabs. The fiducial mass is 40 kton i.e. the detector can be accommodated in one of the existing LNGS experimental halls. The RPC are housed in a 2 cm gap and the signal is readout on external pick-up electrodes segmented in  $2 \times 2 \text{ cm}^2$  pads. This detector can be divided into large modules (about 15 m length) and magnetized by copper coils running through the slabs. This design, which resembles the toroidal configuration of MINOS, was studied in detail by the

<sup>3</sup> ${}^6\text{He}$  and  ${}^{18}\text{Ne}$  having nearly the same Q-value, equal  $\gamma$  corresponds to equal average neutrino energy.

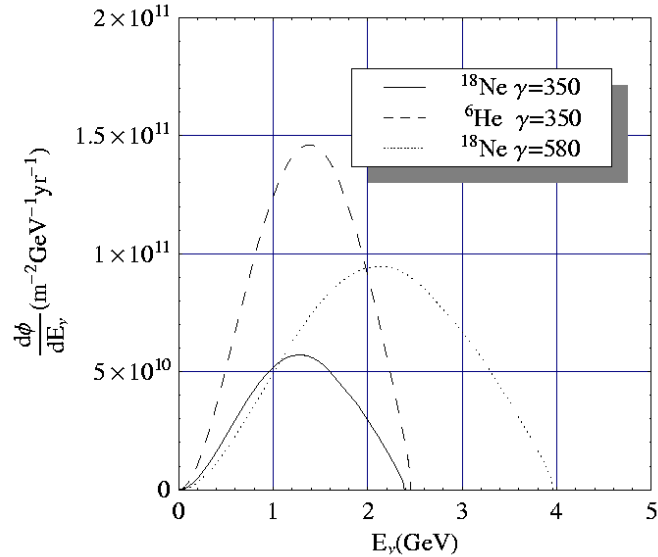


Figure 4: Neutrino spectra at the far location.

MONOLITH Collaboration in 1999 [28] and it has been recently revived by the Indian proposal INO [29, 30]. Hence, the far detector of [12] represents a unique atmospheric neutrino detector. In particular, MONOLITH studies<sup>4</sup> have demonstrated that the vertical orientation of the steel does not compromise the capability of reconstructing the oscillation pattern of atmospheric neutrinos. Moreover, the atmospheric analysis profits of the higher granularity needed for the accelerator-based  $\nu_\mu$  appearance search.

In the following, we consider a 40 kton magnetized detector running at a Beta Beam for 10 years. The accelerator facility is assumed to provide  $2.9 \times 10^{18}$   $^6\text{He}$  and  $1.1 \times 10^{18}$   $^{18}\text{Ne}$  decays per year. As in Ref. [12], we stress that no solid estimate of fluxes are available for the Super-SPS option: we refer to [12] for a systematic study of the sensitivity as a function of fluxes.

## 4 Analysis of atmospheric data

The simulation of atmospheric events at the far detector for the Beta Beam is similar to the one recently implemented by MINOS [31]: flux expectations are based on the Bartol 96 [32] model and interactions have been calculated with GRV94 [33] parton distributions including contributions from quasi-elastic and single pion production [25]. The detector response has been fully simulated with GEANT3 [34] assuming the magnetic field maps resulting from the coil arrangement of MONOLITH. The average magnetic field along the slabs is  $\sim 1.3$  T.

<sup>4</sup>The interest for a vertical slab configuration was originally motivated by the possible exploitation of MONOLITH at CNGS (see Ref.[28] Chap.2).

As discussed in Sec. 2, a substantial enhancement of the sensitivity to hierarchy can be obtained tuning the event selection to identify the region where resonant enhancement occurs. The resonance appears as a perturbation to the original  $L/E$  pattern for a given earth matter density. For  $\cos\theta > 0.85$  the neutrinos cross the earth core and resonant conversions can appear already at few GeV ( $E_R \simeq 3$  GeV). At smaller  $\cos\theta$   $\nu$ 's intersects the Earth mantle and crust and resonances appear at larger  $E_R$  ( $\sim 7$  and  $\sim 11$  GeV respectively). Hence, a two dimensional analysis either in  $E$  versus  $L$  or, equivalently, in  $L/E$  versus  $\cos\theta$  is appropriate to extract information on the existence and location of Earth matter resonances. The choice of  $L/E$  a variable allows the implementation of the Monolith criteria for the observability of the sinusoidal pattern [28] to the search for resonant conversion. This approach has been developed in [25], where the expected resolution on  $L$  and  $E$  is computed on an event-by-event basis; here, events are retained only if the expected resolution is adequate (FWHM on  $L/E$  smaller than 50%) in the region of interest for matter effect perturbations. A preselection is applied requiring a minimum muon energy of 1.5 GeV; only internal events are considered: they can be either fully contained or with a single outgoing track ranging out of the detector with a visible path-length greater than 4 m. On average, these requirements result in a selection efficiency that is negligible below 3 GeV and nearly constant ( $\sim 55\%$ ) above 5 GeV. At these energies, charge misidentification is well below 5% and therefore, rather pure  $\mu^+$  and  $\mu^-$  samples can be collected.

Fig. 5 (left) shows the  $L/E$  distribution of selected events corresponding to 400 kton·year (10 y of data taking) for  $\Delta m_{31}^2 = 2.5 \cdot 10^{-3} \text{ eV}^2$ ,  $\sin^2 2\theta_{13} = 0.1$  and  $\theta_{23} = 45^\circ$ . In this figure, also down-going events are shown: they are used as an unoscillated reference sample to reduce the systematics due to the uncertainty on the initial fluxes. The ratio upgoing/downgoing is shown in Fig. 5 (right); the fit assumes  $\theta_{13} = 0^\circ$ : perturbations due to matter effects and finite  $\theta_{13}$  are visible only for neutrinos since normal hierarchy is assumed; moreover, distortion with respect to pure  $\nu_\mu \rightarrow \nu_\tau$  oscillations are present mainly beyond the first minimum of the survival probability.

## 5 Sensitivity to mass hierarchy

The determination of mass hierarchy from atmospheric neutrinos is plagued by the uncertainty on the mixing parameters, particularly on  $\theta_{13}$ . Accelerator neutrino experiments (a Beta Beam in the present case) can provide very strong constraints on this angle, once marginalized over  $\delta$ . In particular, the manifold of the allowed  $\theta_{13}, \delta$  values is highly reduced by running both in  $\nu_e \rightarrow \nu_\mu$  and in its CP-conjugate mode (anti-neutrino run). Hence the combination of accelerator and atmospheric data can be rather effective [9, 10].

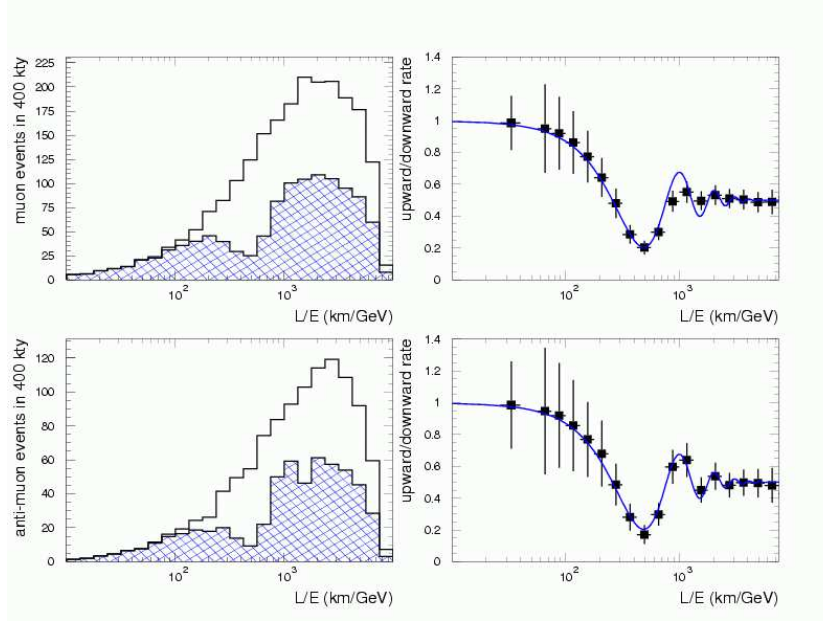


Figure 5:  $L/E$  distribution of selected events corresponding to 400 kton-year (10 y of data taking) for  $\Delta m_{31}^2 = 2.5 \cdot 10^{-3} \text{ eV}^2$ ,  $\sin^2 2\theta_{13} = 0.1$  and  $\theta_{23} = 45^\circ$  (left upper: neutrinos, left lower: antineutrinos). The shaded (unshaded) histogram corresponds to the sample of up-going (down-going) neutrinos. For illustration of the effect, the ratio upgoing/downgoing is also shown (right) together with a fit that assumes  $\theta_{13} = 0^\circ$ .

## 5.1 Likelihood analysis

The analysis of accelerator data employed in the following does not differ from the one described in [12]: we refer to that reference for the details of event selection and detector performance. The sensitivity to the sign of  $\Delta m_{31}^2$  is computed from a likelihood analysis that combines the allowed  $\theta_{13}$  range resulting from the Beta Beam run with the atmospheric likelihood:

$$\ln \mathcal{L} = \ln \prod_{i,q} \left[ \frac{e^{-A_q \mu_{i,q}} (A_q \mu_{i,q})^{U_{i,q}}}{U_{i,q}!} \right] - \sum_q \frac{1}{2} \frac{(A_q - 1)^2}{\sigma_A^2} \quad (3)$$

where the subscripts  $i$  and  $q$  are referred to bins in the  $(\cos \theta, L/E)$  plane and of muon charge respectively;  $U_{i,q}$  and  $A_q \mu_{i,q}$  are the observed and expected number of up-going neutrino events in the  $i, q$ -th bin and the last term in the likelihood accounts for the overall normalization uncertainty for neutrinos and anti-neutrinos separately: further details on the treatment of systematics and their relevance for the mass hierarchy determination are provided below (Sec. 5.2). Additional penalty terms of the form  $(P - P_{best})^2/2\sigma^2$  are added to (3) to account for the uncertainty on  $P = |\Delta m_{31}^2|$  and  $P = \theta_{23}$ . Here,  $P_{best}$  is the current best estimate of the parameter and  $\sigma$  the estimated precision. The latter is the current precision for  $\theta_{23}$  and the expected one at the end

of T2K for  $|\Delta m_{31}^2|$ . For each “true” value of  $\theta_{13}$ ,  $\delta$  and the sign of  $\Delta m_{31}^2$  (e.g. +1 for normal hierarchy), we compute the C.L. of the best fit for the wrong hypothesis (e.g.  $\text{sign}(\Delta m_{31}^2) = -1$ ). Fig. 6 shows the region where the wrong hypothesis is excluded at 90, 95 and 99% C.L. This figure demonstrates what stated qualitatively in Sec. 2: due to the insensitivity to the Dirac phase, the cancellation effect that equals the rates of  $\mu^+$  and  $\mu^-$  at the Beta Beam does not take place with atmospheric. Hence, atmospheric data are relevant and, actually, dominate the sensitivity to mass hierarchy in most of the Beta Beam blind region. In the present scenario, hierarchy can be determined at 90% C.L. down to  $\theta_{13} \simeq 4^\circ$ . At positive (negative)  $\delta$  and normal (inverted) hierarchy, the Beta Beam data dominates and  $\text{sign}(\Delta m_{31}^2)$  can be extracted down to  $\theta_{13} \simeq 2^\circ$ . Compared with stand-alone analysis of atmospheric neutrinos with high density detectors [25], where some sensitivity can be achieved only for  $\theta_{13}$  values very close to current CHOOZ limits, here the accelerator-based determination of this parameter pushes the sensitivity to the mass hierarchy down to  $\sin^2 2\theta_{13} \simeq 0.02$  even for very unfavorable values of the Dirac phase  $\delta$ . This is illustrated in Fig. 7 where the likelihoods for the atmospheric sample only are shown for  $\theta_{13} = 5^\circ$ . The left (right) plots assume normal (inverted) hierarchy as the true hierarchy. In general, Fig. 7 shows that hierarchy separation cannot be achieved if  $\theta_{13}$  is completely unconstrained: on the other hand, even for the most unfavorable values of  $\delta$ , the Beta Beam provides stringent limits to  $\theta_{13}$  that makes the atmospheric sample a sensitive tool for hierarchy determination. If the true hierarchy is inverted, distortions will appear in the antineutrino sample, i.e. in the atmospheric sample with lower statistics due to the difference between  $\nu_\mu$  and  $\bar{\nu}_\mu$  cross sections. However, the discrimination power depends on the difference between the higher statistics  $\nu_\mu$  sample and the lower statistics  $\bar{\nu}_\mu$  one and, as visible from Fig. 7, the power of the test is practically the same both assuming normal and inverted “true” hierarchy.

The use of the Monolith criteria for event selection improves substantially the sensitivity with respect to analyses where flat resolutions have been assumed [16]. In spite of their limited mass, high density atmospheric detectors compete with megaton-size water Cherenkov’s thanks to the capability of measuring the sign of the multi-GeV sample. On the other hand, due to larger statistics, accelerator data are sensitive to perturbations induced by the sign of  $\Delta m^2$  up to  $\sin^2 2\theta_{13} \simeq 0.03 - 0.02$  (see Fig.16 of Ref.[10]). Finally, it is worth noting that significantly better results (sensitivities to the hierarchy down to  $\sin^2 2\theta_{13} < 0.01$ ) could be achieved by dedicated detectors located at the magic baseline without the use of atmospheric sample [14]. These setups, however, requires either large boosters for the beta-beam ions (LHC) or novel ions with larger Q-values and increased flux to compensate for the losses at the far location [15]. Moreover, no information on CP violation in the leptonic sector would be accessible and a second detector at a closer distance from the source would be needed.

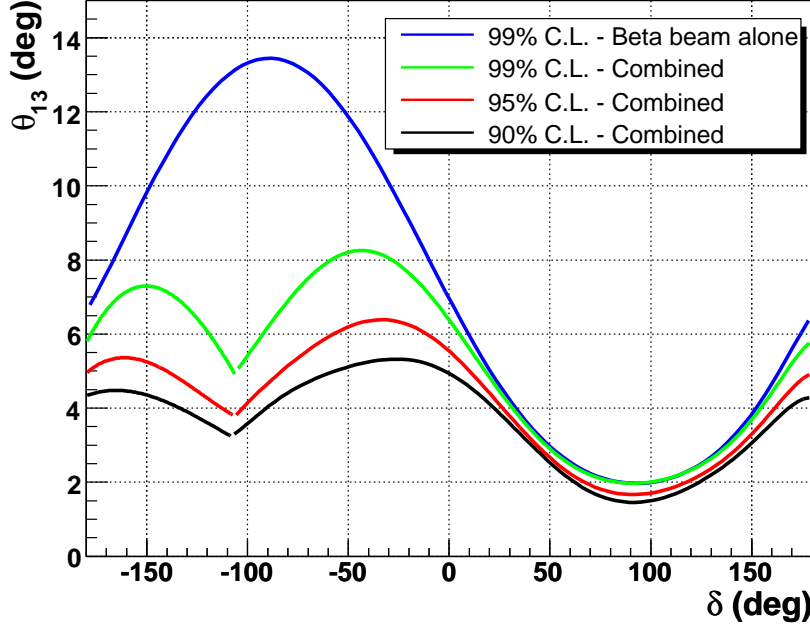


Figure 6: Region of the true value of the parameters  $\theta_{13}$  and  $\delta$  where the correct neutrino hierarchy (assumed to be normal in this figure) can be distinguished from the wrong one at 90, 95 and 99% C.L. Data from the Beta Beam only are also shown.

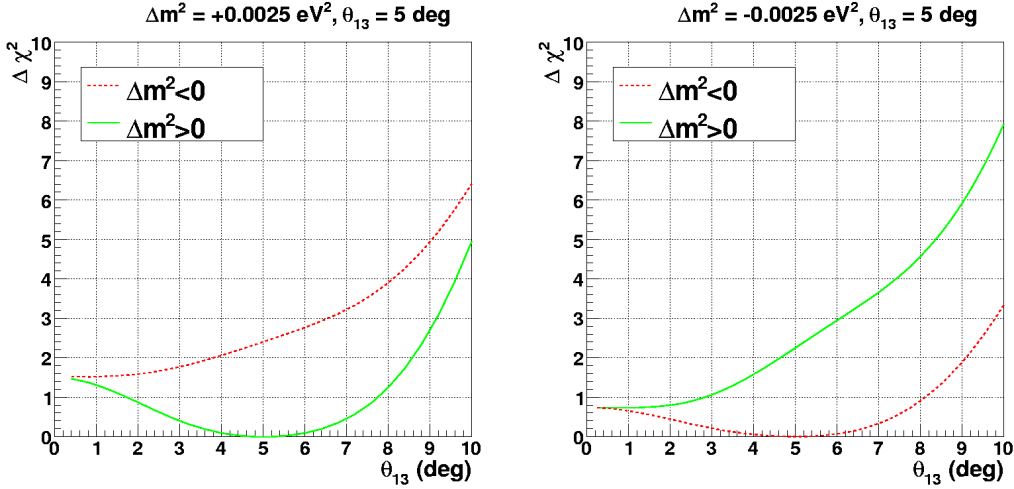


Figure 7: Likelihoods of the atmospheric sample ( $\Delta\chi^2 \equiv -2\text{Log}(L/L_{max})$ ) as a function of  $\theta_{13}$  assuming normal hierarchy (left plot) or inverted hierarchy (right plot) as true hierarchy and  $\theta_{13} = 5^\circ$ . The continuous green line is the likelihood for  $\Delta m^2 > 0$  (right hypothesis in the left plot, wrong hypothesis in the right plot) and the dashed red line is for  $\Delta m^2 < 0$ .

## 5.2 Systematic uncertainties for the atmospheric sample

Systematic uncertainties on the rate of multi-GeV and sub-GeV samples of atmospheric neutrinos have been studied in depth in literature due to their relevance for the determination of the leading oscillation parameters  $\Delta m_{13}$  and  $\sin^2 \theta_{23}$ . Moreover, they affect the pattern of muon disappearance and the perturbation of the  $\nu_e$  sample and, therefore, they can be limiting factors in the determination of the mass hierarchy and  $\theta_{13}$ . In our case, the knowledge of  $\theta_{13}$  is completely dominated by accelerator data while the determination of the mass hierarchy is mainly related to the location of the MSW resonance in the neutrino or antineutrino sample. Hence, several systematic contributions that currently limit the knowledge of the leading parameters at atmospheric detectors (overall flux and cross section normalization,  $\nu_\mu/\nu_e$  ratio, zenith and energy dependence of the differential fluxes) play here a minor role. In order to probe quantitatively such statement, in the present analysis systematics uncertainties have been treated following the approach developed by the Monolith collaboration and based on up-down differential normalization [28, 35]. For each bin in the  $L/E$  distribution of the up-going neutrinos, the unoscillated sample is taken from the corresponding down-going. Here “up-going” means that neutrinos reach the detector coming from below the horizon ( $\cos \theta > 0$ ); the “corresponding down-going” are neutrinos whose Nadir angle  $\theta'$  is such that  $\theta' = \pi - \theta$ . This subsample provides a nearly theory-free normalization since the uncertainties on the flux and cross sections affecting the population of such bin cancel out because of the spherical symmetry and the isotropy of the primary cosmic ray flux. Further details and interesting subtleties can be found in the Monolith proposal [28]. For instance, geomagnetic effects can introduce an asymmetry in the up/down sample that could be interpreted as a perturbation of the  $L/E$  pattern. However, for the multi-GeV sample selected in this analysis, with a minimum neutrino energy of 3 GeV (see Sec. 4), this effect is negligible [36]. Yet, an overall penalty term in the flux normalization has been introduced (see Eq. 3), to cope with the  $\nu_\mu/\nu_e$  ratio uncertainty, as the proposed detector cannot directly measure the  $\nu_e$  flux. This approach is somewhat conservative: in most of the cases, the present theoretical knowledge of the atmospheric fluxes exceed the statistical precision of the down-going samples for bin widths comparable to the detector resolution. However, for the present case where systematics play a less important role than for the leading parameter analysis, this technique simplifies remarkably the treatment of systematics without compromising the sensitivity to the mass hierarchy. To ease comparison with other analyses (See e.g. Table 1 of [16]) we note that the statistical uncertainty of the down-going sample in the region where the oscillation dip at  $\theta_{13}$  is located is of about 9%, while typical differential uncertainties in the rate of multi-GeV  $\nu_\mu$  are of the order of 5%. Moreover, the down-going normalization sample is measured for neutrinos and antineutrinos separately, hence assuming that the uncertainty on the  $\nu_\mu/\bar{\nu}_\mu$  ratio could also have a dependence in energy and in direction, while in most of the analyses a flat uncertainty of about 5% is considered. As a consistency check, we artificially decreased the statistical uncertainty of the down-going sample up to 3% noting that

the sensitivity to the sign of  $\Delta m_{31}^2$  remains practically unchanged. This is in agreement to what already observed by some authors, i.e. that “the discrimination between normal and inverted hierarchy is based on a very characteristic signal consisting of pronounced structures in the  $E$  and  $\cos \theta$  distributions, which cannot easily mimicked by the systematic effects” [16].

The most relevant systematic uncertainty of instrumental origin is related to the pollution of the neutrino sample with antineutrinos due to charge misassignment. In most of the analyses presented in literature, an overall uncertainty on the knowledge of the charge (typically of 5%) is assumed independently of the topology of event. The present analysis, instead, is based on a full GEANT3 simulation of the detector, followed by a reconstruction stage with track fitting. Neutrino flavour assignment is based on the reconstructed muon charge, thus encompassing a realistic energy and event shape dependency, as far as GEANT3 can predict the behaviour of magnetised iron calorimeters<sup>5</sup>. The charge misidentification systematics is the most relevant detector-dependent systematics in the atmospheric analysis, while it is immaterial in the Beta Beam analysis, where  $\pi/\mu$  misidentification dominates. This is the reason why we assumed the systematics of the accelerator and atmospheric data fully uncorrelated.

## 6 Conclusions

Detailed atmospheric neutrino studies can be done in several detectors that have been built or proposed for long-baseline accelerator facilities. In particular, high density magnetized detectors can study multi-GeV atmospheric neutrinos and distinguish between  $\nu_\mu$  and  $\bar{\nu}_\mu$ . These data can be combined in a highly non trivial manner to improve the sensitivity to the neutrino mass hierarchy. In this paper we considered in particular a high energy Beta Beam with a 40 kton iron calorimeter located at the CERN to Gran Sasso distance. The atmospheric data collected by this detector allows the determination of the neutrino hierarchy down to  $\theta_{13} \simeq 4^\circ$  in the region of  $\delta$  where the corresponding Beta Beam data cannot constrain the sign of  $\Delta m_{31}^2$ . Far from this blind region, the Beta Beam data dominates and  $\text{sign}(\Delta m_{31}^2)$  can be extracted down to  $\theta_{13} \simeq 2^\circ$  at 90% C.L.

## Acknowledgments

We wish to express our gratitude to S. Petcov, S. Agarwalla and A. Blondel for several useful discussions during the WIN07 workshop in Kolkata.

---

<sup>5</sup>Solid testbeds are based, e.g., on the CDHS and MINOS data, on non-compensated hadronic calorimeters at colliders and on Monolith testbeams [37].

## References

- [1] W. M. Yao *et al.* [Particle Data Group], J. Phys. G **33** (2006) 1 and references therein.
- [2] Q.R. Ahmad *et al.* [SNO Coll.], Phys. Rev. Lett. **87** (2001) 071301; B. Aharmim *et al.* [SNO Collaboration], Phys. Rev. C **72** (2005) 055502; T. Araki *et al.* [KamLAND Collaboration] Phys. Rev. Lett. **94** (2005) 081801; Y. Ashie *et al.* [Super-Kamiokande Collaboration], Phys. Rev. D **71** (2005) 112005; M. Ambrosio *et al.* [MACRO Collaboration], Phys. Lett. B **566** (2003) 35; . Aliu *et al.* [K2K Collaboration], Phys. Rev. Lett. **94** (2005) 081802. K. Abe *et al.* [Super-Kamiokande Collaboration], Phys. Rev. Lett. **97** (2006) 171801; J. Hosaka *et al.* [Super-Kamiokande Collaboration], Phys. Rev. D **74** (2006) 032002; D. G. Michael *et al.* [MINOS Collaboration], Phys. Rev. Lett. **97** (2006) 191801.
- [3] R. Acquafredda *et al.* [OPERA Collaboration], New J. Phys. **8** (2006) 303.
- [4] M. Apollonio *et al.* [CHOOZ Collaboration], Eur. Phys. J. C **27** (2003) 331; M. Apollonio *et al.* [CHOOZ Collaboration], Phys. Lett. B **466** (1999) 415; F. Boehm *et al.* [Palo Verde Collaboration], Phys. Rev. D **64** (2001) 112001.
- [5] For a review see A. Guglielmi, M. Mezzetto, P. Migliozzi and F. Terranova, arXiv:hep-ph/0508034 (in D. Bettoni *et al.*, Phys. Rep. **434** (2006) 47, pp.68-87).
- [6] S. Geer, Phys. Rev. D **57** (1998) 6989 [Erratum-ibid. D **59** (1999) 039903]; A. De Rujula, M. B. Gavela and P. Hernandez, Nucl. Phys. B **547** (1999) 21.
- [7] P. Zucchelli, Phys. Lett. B **532** (2002) 166.
- [8] J. Bernabeu, S. Palomares Ruiz and S. T. Petcov, Nucl. Phys. B **669** (2003) 255; M. C. Gonzalez-Garcia and M. Maltoni, Eur. Phys. J. C **26** (2003) 417; M. C. Gonzalez-Garcia, M. Maltoni and A. Y. Smirnov, Phys. Rev. D **70** (2004) 093005
- [9] P. Huber, M. Maltoni and T. Schwetz, Phys. Rev. D **71** (2005) 053006.
- [10] J. E. Campagne, M. Maltoni, M. Mezzetto and T. Schwetz, JHEP **0704** (2007) 003.
- [11] J. Burguet-Castell, D. Casper, J. J. Gomez-Cadenas, P. Hernandez and F. Sanchez, Nucl. Phys. B **695** (2004) 217; J. Burguet-Castell, D. Casper, E. Couce, J. J. Gomez-Cadenas and P. Hernandez, Nucl. Phys. B **725** (2005) 306.
- [12] A. Donini, E. Fernandez-Martinez, P. Migliozzi, S. Rigolin, L. Scotto Lavina, T. Tabarelli de Fatis and F. Terranova, Eur. Phys. J. C **48** (2006) 787

- [13] P. Huber, M. Lindner, M. Rolinec and W. Winter, Phys. Rev. D **73** (2006) 053002; F. Terranova, A. Marotta, P. Migliozzi and M. Spinetti, Eur. Phys. J. C **38** (2004) 69.
- [14] S. K. Agarwalla, A. Raychaudhuri and A. Samanta, Phys. Lett. B **629** (2005) 33; S. K. Agarwalla, S. Choubey and A. Raychaudhuri, Nucl. Phys. B **771** (2007) 1.
- [15] C. Rubbia, A. Ferrari, Y. Kadi and V. Vlachoudis, Nucl. Instrum. Meth. A **568** (2006) 475; A. Donini and E. Fernandez-Martinez, Phys. Lett. B **641** (2006) 432.
- [16] S. T. Petcov and T. Schwetz, Nucl. Phys. B **740** (2006) 1
- [17] C. H. Albright and M. C. Chen, Phys. Rev. D **74** (2006) 113006.
- [18] A. de Gouvea, J. Jenkins and B. Kayser, Phys. Rev. D **71** (2005) 113009; H. Minakata, H. Nunokawa, S. J. Parke, R. Zukanovich Funchal, Phys. Rev. D **74** (2006) 053008; H. Minakata, H. Nunokawa, S. J. Parke and R. Z. Funchal, Phys. Rev. D **76** (2007) 053004 [Erratum-ibid. D **76** (2007) 079901].
- [19] A. Cervera et al., Nucl. Phys. B **579** (2000) 17, erratum ibid. Nucl. Phys. B **593** (2001) 731.
- [20] M. Freund, Phys. Rev. D **64** (2001) 053003.
- [21] O. Bruning et al., “LHC luminosity and energy upgrade: A feasibility study,” CERN-LHC-PROJECT-REPORT-626, 2002; W. Scandale, Nucl. Phys. Proc. Suppl. **154** (2006) 101.
- [22] D. S. Ayres *et al.* [NOvA Collaboration], arXiv:hep-ex/0503053.
- [23] V. Barger, D. Marfatia and K. Whisnant, Phys. Rev. D **65** (2002) 073023; P. Huber and W. Winter, Phys. Rev. D **68** (2003) 037301.
- [24] A. Y. Smirnov, arXiv:hep-ph/0610198.
- [25] T. Tabarelli de Fatis, Eur. Phys. J. C **24** (2002) 43.
- [26] A.M. Dziewonski and D.L. Anderson, Phys. Earth Planet. Inter., **25** (1981) 297
- [27] M. Benedikt, A. Fabich, S. Hancock, M. Lindroos, EURISOL DS/TASK12/TN-05-03.
- [28] N.Y. Agafonova *et al.* [MONOLITH Collaboration], LNGS-P26-2000, LNGS-P26-00, CERN-SPSC-2000-031, CERN-SPSC-M-657.
- [29] M. S. Athar *et al.* [INO Collaboration], “India-based Neutrino Observatory: Project Report. Vol.I,” , INO-2006-01.

- [30] R. Gandhi, P. Ghoshal, S. Goswami, P. Mehta and S. Uma Sankar, Phys. Rev. D **73** (2006) 053001.
- [31] P. Adamson *et al.* [MINOS Collaboration], Phys. Rev. D **75** (2007) 092003.
- [32] V. Agrawal, T.K. Gaisser, P. Lipari and T. Stanev, Phys. Rev. D **53** (1996) 1314.
- [33] M. Gluck, E. Reya and A. Vogt, Z. Phys. C **67** (1995) 433.
- [34] GEANT - Detector Description and Simulation Tool CERN Program Library Long Writeup W5013.
- [35] P. Picchi and F. Pietropaolo, ICGF Internal Note 344/1997, available as CERN Preprint SCAN, SCAN-9710037.
- [36] V. Agrawal, T. K. Gaisser, P. Lipari and T. Stanev, Phys. Rev. D **53** (1996) 1314.
- [37] M. Ambrosio *et al.*, Nucl. Instrum. Meth. A **456** (2000) 67.